

Time Delay Extraction from Frequency Domain Data Using Causal Fourier Continuations for High-Speed Interconnects

Lyudmyla L. Barannyk¹, Hung H. Tran², Aicha Elshabini², and Fred D. Barlow³

Abstract—We present a new method for time delay estimation using band limited frequency domain data representing the port responses of interconnect structures. The approach is based on the recently developed by the authors spectrally accurate method for causality characterization that employs SVD-based causal Fourier continuations. The time delay extraction is constructed by incorporating a linearly varying phase factor to the system of equations that determines Fourier coefficients. The method is capable of determining time delay using data affected by noise or approximation errors that come from measurements or numerical simulations. It can also be employed when only a limited number of frequency responses is available. The technique can be extended to multi-port and mixed mode networks. Several analytical and simulated examples are used to demonstrate the accuracy and strength of the proposed technique.

Index Terms—time delay, delay estimation, causality, dispersion relations, singular value decomposition, SVD-based causal Fourier continuation, high speed interconnects.

I. INTRODUCTION

Identification and extraction of time delay is an important research problem in signal processing and has applications in many fields including radar [25], sonar [33], [8], ultrasonics [10], microwave imaging [26], geophysics [22], seismology [39], [29], wireless communications [36] as well as modeling of passive structures in electronic systems, in particular, transmission line modeling [18], [11], transient simulation of interconnects [24] and co-simulation of passive structures with active devices in a time domain using SPICE. Passive structures in electronic systems have been traditionally analyzed in the frequency domain, while transient simulations are performed in the time domain using suitable models that accurately capture the relevant electromagnetic phenomena. The models are obtained from either direct measurements or electromagnetic simulations. Interconnect models are typically approximated by rational transfer functions using the vector fitting algorithm in various implementations [19], [15], [20], [12], [17], [13], [9], which is the standard macromodeling approach. As clock frequencies increase, the size of passive structures becomes of the same order as the signal wavelength at the operating frequency, which causes the distributed effects

such as time delay to play a significant role in the time domain simulations. For this reason, time delay has to be included in macromodeling, in particular, when causality is analyzed. The connection between causality and time delay is in the fact that time delays can pull a non-causal signal into the causal region or vice versa pull a causal signal into the non-causal region, while causality, in turn, can be expressed in terms of the Hilbert transform [32], [38], [31]. Several approaches can be used to extract delays in the frequency domain, for example, using the Hilbert transform [14], [35], [23], the minimum phase all-pass decomposition [28], [27], [24], incorporating an optimal time delay into the vector fitting algorithm [18], [11], employing a modified Lie approximation to develop a passive and compact macromodel [30], using a Gabor transform to develop delayed rational function macromodels for long interconnects [16], [9] or conducting a probabilistic analysis of the cepstrum in the presence of noise [21]. In the time domain, delayed rational functions [7], [6] can be employed to extract delays. In this paper, a novel approach is proposed in which time delay is determined in the frequency domain using a causality argument. Causality is verified using the SVD-based causal Fourier continuation method developed by the authors [4], [2], while the time delay presence is incorporated by a linearly varying phase factor to the system of equations that determines Fourier coefficients. Preliminary results are reported in [5].

The rest of the paper is organized as follows. Section II provides a background on causality for linear time-translation invariant systems and dispersion relations. In Section III, we show main steps in the derivation of causal Fourier continuations using truncated singular value decomposition (SVD) method that was developed to access causality. We also provide error estimates that take into account a possible presence of noise in data. Section IV extends the causality characterization method to develop a technique for time delay extraction. The proposed method is tested in Section V using several analytic and simulated examples. We also analyze the performance of the algorithm when only a limited number of frequency responses is available and when noise/approximation errors are present in data. In Section VI we present our conclusions. The Appendix section is devoted to formulation of error bounds for the causality characterization method based on causal Fourier continuations.

Lyudmyla L. Barannyk is with the Department of Mathematics, University of Idaho, Moscow, Idaho 83844, USA (e-mail: barannyk@uidaho.edu).

Hung H. Tran and Aicha Elshabini are with the Department of Electrical & Computer Engineering, University of Idaho, Moscow, Idaho 83844, USA (e-mails: tran4105@vandals.uidaho.edu; elshabini@uidaho.edu).

Fred Barlow is with the College of Engineering, University of Alaska Anchorage, Anchorage, Alaska 99508, USA (e-mail: fdbarlow@uaa.alaska.edu).

II. CAUSALITY OF LINEAR TIME-INVARIANT SYSTEMS

Consider a linear and time-invariant physical system with the impulse response $h(t)$ subject to a time-dependent input $f(t)$, to which it responds by an output $x(t)$. Denote by

$$H(w) = \int_{-\infty}^{\infty} h(\tau) e^{-iw\tau} d\tau \quad (1)$$

the Fourier transform of $h(t)$, which is also called the transfer function.

The system is causal if the output cannot precede the input, i.e. if $f(t) = 0$ for $t < T$, the same must be true for $x(t)$. This primitive causality condition in the time domain implies $h(t) = 0, t < 0$. Hence, domain of integration in (1) can be reduced to $[0, \infty)$.

Assume $H(w) \in L_2(\mathbb{R})$. Then starting from Cauchy's theorem and using contour integration, one can show [31] that for any point w on the real axis, $H(w)$ can be written¹ as

$$H(w) = \frac{1}{\pi i} \mathcal{P} \int_{-\infty}^{\infty} \frac{H(w')}{w - w'} dw', \quad \text{real } w, \quad (2)$$

where

$$\mathcal{P} \int_{-\infty}^{\infty} = P \int_{-\infty}^{\infty} = \lim_{\epsilon \rightarrow 0} \left(\int_{-\infty}^{w-\epsilon} + \int_{w+\epsilon}^{\infty} \right)$$

denotes Cauchy's principal value. Separating the real and imaginary parts of (2), we get

$$\text{Re } H(w) = \frac{1}{\pi} \mathcal{P} \int_{-\infty}^{\infty} \frac{\text{Im } H(w')}{w - w'} dw', \quad (3)$$

$$\text{Im } H(w) = -\frac{1}{\pi} \mathcal{P} \int_{-\infty}^{\infty} \frac{\text{Re } H(w')}{w - w'} dw'. \quad (4)$$

Expressions (3) and (4) are called the dispersion relations or Kramers-Krönig relations. They show that $\text{Re } H$ and $\text{Im } H$ are not independent functions, but instead they are related to each other: $\text{Re } H$ at one frequency depends on $\text{Im } H$ at all frequencies, and vice versa. This implies that if one of the functions $\text{Re } H$ or $\text{Im } H$ is square integrable and known, then the other one can be completely determined by causality. Recalling the definition of the Hilbert transform,

$$\mathcal{H}[u(w)] = \frac{1}{\pi} \mathcal{P} \int_{-\infty}^{\infty} \frac{u(w')}{w - w'} dw',$$

we see that $\text{Re } H$ and $\text{Im } H$ are Hilbert transforms of each other, i.e.

$$\text{Re } H(w) = \mathcal{H}[\text{Im } H(w)], \quad \text{Im } H(w) = -\mathcal{H}[\text{Re } H(w)]. \quad (5)$$

In other words, $\text{Re } H$ or $\text{Im } H$ form a Hilbert transform pair. Dispersion relations provide the causality condition in the frequency domain.

Evaluation of the Hilbert transform requires integration on $(-\infty, \infty)$, which can be reduced to $[0, \infty)$ by spectrum symmetry of $H(w)$ if $h(t)$ is real valued. In practice, only a limited number of discrete values of $H(w)$ is available on $[w_{min}, w_{max}]$. Thus, the domain of integration has to be truncated. This usually causes serious boundary artifacts due to

the lack of out-of-band frequency responses. To reduce or even completely remove boundary artifacts, the authors recently developed periodic polynomial [1], [3] and causal Fourier continuation [2], [4], respectively, based methods for causality characterization. The approach was motivated by the example $H(w) = e^{-iaw}, a > 0$, that is not square integrable but still satisfies the dispersion relations. The causality characterization method based on causal Fourier continuations allows one to construct highly accurate approximations of a given transfer function on the original frequency interval $[w_{min}, w_{max}]$ with the uniform error that decreases as the number of Fourier coefficients increases. The technique is applicable to both baseband and bandpass cases and capable of detecting very small localized causality violations. The method can also be extended to multidimensional cases.

In the next section, for completeness of presentation, we show main steps in the derivation of the causal Fourier continuation method that can be used to access causality of a given transfer function whose values are available at a discrete set of frequencies. We also provide upper bounds of reconstruction error between the given function and its causal Fourier continuation. We use these error estimates to understand how to extract time delay when data with different resolutions are available and when data are affected by noise or other approximation errors.

III. CAUSAL FOURIER CONTINUATIONS

Consider a transfer function $H(w) = \text{Re } H + i \text{Im } H$, whose N discrete values are available on $[w_{min}, w_{max}]$, $w_{min} \geq 0$. For real-valued impulse response functions $h(t)$, $\text{Re } H$ and $\text{Im } H$ are even and odd functions, respectively. This implies that $H(w)$ has values on $[-w_{max}, -w_{min}]$ by spectrum symmetry. For convenience, we rescale the frequency interval $[-w_{max}, w_{max}]$ to $[-0.5, 0.5]$ by the substitution $x = \frac{0.5}{w_{max}} w$, so the rescaled transfer function $H(x)$ is defined on the unit length interval with \tilde{N} values where $\tilde{N} = 2N - 1$ or $\tilde{N} = 2N$ depending if $H(x)$ is available at $x = 0$ or not. Both baseband and bandpass cases can be considered.

The idea of a causal Fourier continuation is to construct an accurate Fourier series approximation of $H(x)$ by allowing the Fourier series to be periodic and causal in an extended domain. The result is the Fourier continuation of H that we denote by $\mathcal{C}(H)$, and it is defined by

$$\mathcal{C}(H)(x) = \sum_{k=-M+1}^M \alpha_k e^{-\frac{2\pi i}{b} kx}, \quad (6)$$

for even number $2M$ of terms, whereas for odd number $2M+1$ of terms, the index k varies from $-M$ to M . Throughout this paper, we assume that the number M of Fourier coefficients is even, for simplicity. When M is odd, analogous results can be formulated. Here b is the period of approximation. For SVD-based periodic continuations b is normally chosen as twice the length of the domain on which function H is given though the value $b = 2$ is not necessarily optimal. The optimal value b depends on a function being approximated. In practice, several values $b \in (1, 4)$ may be tried to get a better reconstruction of $H(x)$ with a Fourier series.

¹Please note that we use an opposite sign of the exponent in the definition of the Fourier transform than in [31].

Functions $\phi_k(x) = e^{-\frac{2\pi i}{b}kx}$, $k \in \mathbb{Z}$, form a complete orthogonal basis in $L_2[-\frac{b}{2}, \frac{b}{2}]$. It can be shown that $\mathcal{H}\{\phi_k(x)\} = i \operatorname{sgn}(k)\phi_k(x)$, which implies that functions $\{\phi_k(x)\}$ are the eigenfunctions of the Hilbert transform \mathcal{H} with associated eigenvalues $\pm i$ with $x \in [-\frac{b}{2}, \frac{b}{2}]$. For a causal periodic continuation, according to (5), we need $\operatorname{Im} \mathcal{C}(H)(x)$ to be the Hilbert transform of $-\operatorname{Re} \mathcal{C}(H)(x)$. It can be shown [4] that this implies $\alpha_k = 0$ for $k \leq 0$ in (6). Hence, a causal Fourier continuation has the form

$$\mathcal{C}(H)(x) = \sum_{k=1}^M \alpha_k \phi_k(x). \quad (7)$$

Evaluating $H(x)$ at points x_j , $j = 1, \dots, \tilde{N}$, $x_j \in [-0.5, 0.5]$, produces a complex valued system

$$\sum_{k=1}^M \alpha_k \phi_k(x_j) = H(x_j) \quad (8)$$

with \tilde{N} equations for M unknowns α_k , $k = 1, \dots, M$, $\tilde{N} \geq M$. If $\tilde{N} > M$, the system (8) is overdetermined and has to be solved in the least squares sense. When Fourier coefficients α_k are computed, formula (7) provides reconstruction of $H(x)$ on $[-0.5, 0.5]$. The least squares problem is extremely ill-conditioned. However, it can be regularized using a truncated SVD method when singular values below some cutoff tolerance ξ close to the machine precision are being discarded. To have a better control on ill-conditioning of matrix problem (8), more data points \tilde{N} than the Fourier coefficients M should be used. We use at least $\tilde{N} = 2M$ as an effective way to obtain an accurate and reliable approximation of $H(x)$ over the interval $[-0.5, 0.5]$. This relation corresponds² to $N = M$, where N is the number of data points available originally on $[w_{min}, w_{max}]$.

Since $\operatorname{Re} H(x)$ and $\operatorname{Im} H(x)$ are even and odd functions of x , respectively, the Fourier coefficients

$$\alpha_k = \frac{1}{b} \int_{-b/2}^{b/2} H(x) \overline{\phi_k(x)} dx, \quad k = 1, \dots, M,$$

are real. Here $\bar{}$ denotes the complex conjugate. To ensure that numerically computed Fourier coefficients α_k are real, instead of solving complex-valued system (8), one can separate the real and imaginary parts of $\mathcal{C}(H)(x_j)$ to obtain real-valued system

$$\begin{aligned} \operatorname{Re} \mathcal{C}(H)(x_j) &= \sum_{k=1}^M \alpha_k \operatorname{Re} \phi_k(x_j), \\ \operatorname{Im} \mathcal{C}(H)(x_j) &= \sum_{k=1}^M \alpha_k \operatorname{Im} \phi_k(x_j). \end{aligned} \quad (9)$$

We show in [4] that real formulation (9) provides slightly more accurate results than complex.

To access the quality of approximation of $H(x)$ with its causal Fourier continuation $\mathcal{C}(H)(x)$, we introduce reconstruction errors $E_R(x)$ and $E_I(x)$,

$$E_R(x) = \operatorname{Re} H(x) - \operatorname{Re} \mathcal{C}(H)(x), \quad (10)$$

²In [4], N denoted the number of points on $[-0.5, 0.5]$, while in this work N is the number of points on $[0, 0.5]$ or originally on $[w_{min}, w_{max}]$.

$$E_I(x) = \operatorname{Im} H(x) - \operatorname{Im} \mathcal{C}(H)(x) \quad (11)$$

on the original interval $[-0.5, 0.5]$.

The error analysis performed in [4] (see also Appendix) shows that the error between $H(x)$ and its causal Fourier continuation $\mathcal{C}(H + \varepsilon)$ under the presence of a noise ε , has the following upper bound:

$$\|H - \mathcal{C}(H + \varepsilon)\|_{L_2(\Omega)} \leq \epsilon_F + \epsilon_n + \epsilon_T. \quad (12)$$

Here

$$\epsilon_F = (1 + \Lambda_2 \sqrt{2N(M - K)}) \|H - \hat{H}_M\|_{L_\infty(\Omega)} \quad (13)$$

is the error due to approximation of H with a causal Fourier series and it decays as $\mathcal{O}(M^{-k+1})$, where k is the smoothness order of the transfer function $H(x)$.

$$\epsilon_T = \Lambda_1 \sqrt{K/b} \|\hat{H}_M\|_{L_\infty(\Omega^c)} \quad (14)$$

is the error due to the truncation of singular values and it is typically small and close to the cut-off value ξ . As (14) indicates, ϵ_T depends on b and the function H being approximated.

$$\epsilon_n = (1 + \Lambda_2 \sqrt{2N(M - K)}) \|\varepsilon\|_{L_\infty(\Omega)} \quad (15)$$

is the error due to the presence of a noise or approximation errors in the given data and it shows a level of causality violation. In practice the size of ϵ_n is close to the size of noise in data. Function \hat{H}_M and constants Λ_1 , Λ_2 and K are defined in Appendix. These constants depend only on the continuation parameters N , M , b and ξ as well as location of discrete points x_j , and not on the function H .

The error bound (12) shows that the reconstruction errors E_R and E_I decrease as M increases due to the causal Fourier series approximation error with the error bound ϵ_F until either the level ϵ of a noise or level ϵ_T due to truncation of singular values is reached. If only round-off errors are present in data, the errors will level off at ϵ_T . If reconstruction errors level off at some value $\epsilon > \epsilon_T$ as the resolution increases, the data are declared non-causal with the error approximately at the order of ϵ . More information about the error analysis for the causality characterization methods based on causal Fourier continuations can be found in [4].

IV. TIME DELAY ESTIMATION

The above approach for causality assessment can be transformed into a delay estimation algorithm by observing the following. Suppose that $h(t)$ is non-zero only from time $T_0 \geq 0$, and we would like to identify the time delay T_0 . Consider the Fourier transform $H(w)$ of $h(t)$:

$$H(w) = \int_{t=T_0}^{\infty} e^{-iwt} h(t) dt = \int_{t=T_0}^{\infty} e^{-i\frac{x}{a}t} h(t) dt$$

where we used the substitution $x = aw$, $a = \frac{0.5}{w_{max}}$. Introducing $\tau = \frac{t}{a}$, we can write

$$H(w) = a \int_{\frac{T_0}{a}}^{\infty} e^{-ix\tau} h(a\tau) d\tau,$$

or with $u = \tau - \frac{T_0}{a}$, we obtain

$$H(w) = a e^{-ix \frac{T_0}{a}} \int_0^\infty e^{-ixt} h(T_0 + au) du = a e^{-ix \frac{T_0}{a}} G(x),$$

where $G(x)$ is the Fourier transform of a causal function with no time delay. This implies that when $0 \leq T \leq T_0$, the transfer function $H(x) e^{ix \frac{T}{a}}$ is causal, but when $T \geq T_0$, the transfer function $H(x) e^{ix \frac{T}{a}}$ has a non-causal component. Therefore, $\tilde{T}_0 = T_0/a$ is the time delay for $H(x)$, and the delay T_0 for the original function $H(w)$ is recovered by multiplying \tilde{T}_0 by a . Since one can add any integral multiple of 2π to xT/a , it is enough to restrict our investigations to the interval

$$0 \leq \frac{T}{a} \leq T_{max} = \frac{2\pi}{x_{max}} = \frac{2\pi}{0.5} = 4\pi.$$

Then for each potential time delay $0 \leq \frac{T}{a} \leq T_{max}$, we solve the following modified system

$$\sum_{k=1}^M \alpha_k \phi_k(x_j) = e^{ix_j \frac{T}{a}} H(x_j), \quad j = 1, \dots, \tilde{N} \quad (16)$$

or its equivalent real-valued formulation. For $T < T_0$, the reconstruction errors E_R , E_I should be small and approximately of the same order. As T increases and becomes greater than some critical transition time close to the time delay T_0 , the reconstruction errors should start increase. The goal is to approximate T_0 . The difficulty is that the reconstruction errors grow gradually as $T \geq T_0$, so transition is not sharp. Moreover, the order of reconstruction errors for $T < T_0$ depends on the resolution of data and threshold ξ used in the truncated SVD method, which, in turn, affects a transition time. In addition, a noise in data, if present, also affects when reconstruction errors start growing. A similar approach was used in [23] to estimate the time delay for square integrable transfer functions. In this contribution, we extend the approach to more general transfer functions. In addition, we use a different causality measure than in [23] and take into account different resolutions of given data and a possible presence of noise. The approach can be extended to multi-port and mixed mode networks by applying it to each element of the transfer matrix.

V. NUMERICAL EXAMPLES

In this section, we apply a proposed technique to several analytic and simulated examples when the time delay is either known exactly or can be estimated using other techniques. We also consider the effect of noise presence on the accuracy of timed delay estimation.

A. Four-Pole Example

Consider a transfer function with four poles and time delay T_0 , defined by

$$H(w) = e^{-iwT_0} \tilde{H}(w) \quad (17)$$

with

$$\tilde{H}(w) = \frac{r_1}{iw + p_1} + \frac{\bar{r}_1}{iw + \bar{p}_1} + \frac{r_2}{iw + p_2} + \frac{\bar{r}_2}{iw + \bar{p}_2}$$

where $r_1 = 1 + 2i$, $p_1 = 1 + 3i$, $r_2 = \frac{2}{3} + \frac{1}{2}i$, $p_2 = \frac{1}{2} + 5i$, and $T_0 = 0.25$. Since the poles of $\tilde{H}(w)$ are located in the upper half w -plane at $\pm 3 + i$ and $\pm 5 + \frac{1}{2}i$, this function is causal as a sum of four causal transforms, and has no time delay. Therefore, the function $H(w)$ is a causal function delayed with offset T_0 . H is sampled on $[0, w_{max}]$ at N frequency points varying from 50 to 1500 with $w_{max} = 6$. The real and imag-

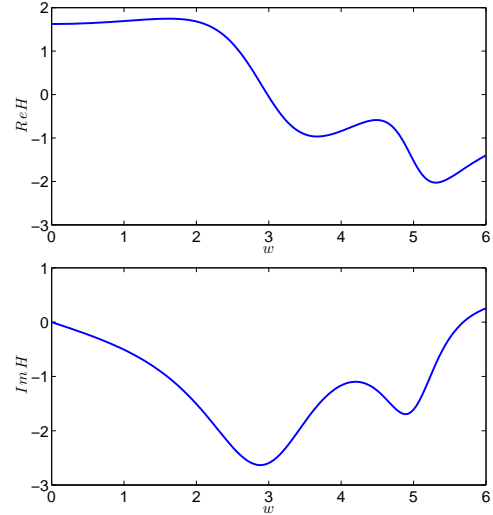


Fig. 1. $\text{Re } H(w)$ and $\text{Im } H(w)$ in the four-pole example.

inary parts of $H(w)$ are shown in Fig. 1. After rescaling with $x = \frac{0.5}{w_{max}} w$ and reflecting to negative frequencies, we obtain a rescaled transfer function $H(x)$ defined on $x \in [-0.5, 0.5]$, for which we construct a causal Fourier continuation $\mathcal{C}(H)$ defined in (7) using $M = N$ Fourier coefficients. Hence, the number M of Fourier coefficients also varies between 50 and 1500. $\text{Re } H(x)$ and $\text{Im } H(x)$ of the rescaled and reflected $H(x)$ together with their causal Fourier continuations with $M = 300$ are depicted in Fig. 2. Even though given $H(x)$ and its causal Fourier continuation approximation look indistinguishable, the actual reconstruction errors E_R and E_I in both real and imaginary parts, that are defined in (10), (11), are on the order of 10^{-6} and they decrease as M increases (with $M = N$). For example, with $M = 800$, the errors are on the order of 10^{-13} . Since both errors E_R and E_I are of the same order, it is enough to analyze one of the errors, for example, E_R . The results using E_I are similar.

To estimate the time delay, we analyze the evolution of the $\|E_R\|_\infty$, shown in Fig. 3, for various values M . Since the error due to a causal Fourier series approximation decreases with M (see error bound (13)), the reconstruction error between the given transfer function H and its causal Fourier continuation $\mathcal{C}(H)$ also decreases as M increases until it either reaches the level ξ of filtering of singular values or a level ϵ of noise/causality violations (see error bounds (14) and (15), respectively). For each fixed M , as time T increases, the errors E_R and E_I first are small and about of the same order until some transition time close to the time delay T_0 is approached. After that the errors grow approximately as a power function on the log scale. For smaller T , the

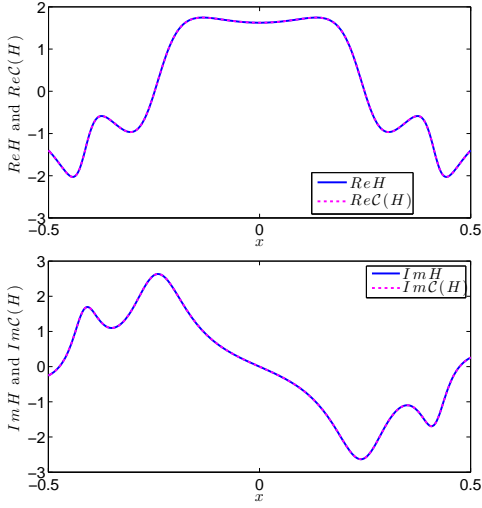


Fig. 2. $\text{Re}H(x)$ and $\text{Im}H(x)$ of the rescaled and reflected by symmetry transfer function $H(x)$ in the four-pole example together with their causal Fourier continuations $\text{Re}C(H)$ and $\text{Im}C(H)$, respectively, with $M = 300$ Fourier coefficients.

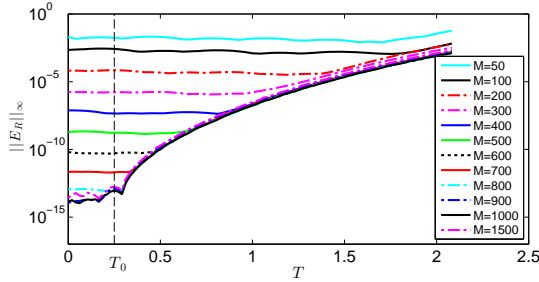


Fig. 3. Evolution of the reconstruction error $\|E_R\|_\infty$ as a function of T in the four-pole example. The dashed line corresponds to the exact delay $T_0 = 0.25$.

errors are dominated by a causal Fourier series approximation error and then for T greater than some transition time – by causality violations since this value T provides large enough negative time delay and shifts a causal function into a non-causal area. A transition value $T = T_c$, we call it a critical time, from a plateau region to a growth region, is different for each M and it decreases as the resolution or number of Fourier coefficients increases if the error is dominated by the causal Fourier series approximation error. The critical times T_c approach the time delay T_0 as M increases. The goal is to estimate T_0 using the error curves shown in Fig. 3. Analyzing graphs of the error curves for $M > 800$, we observe some non-monotonic behavior at T close to T_0 . This behavior is due to the filtering of the singular values below the threshold $\xi = 10^{-13}$ that we used in our experiments. By increasing the value of ξ , the non-monotonic behavior will be present at smaller values of M . This suggests that portions of error curves close to threshold ξ are affected by filtering and may be inaccurate and difficult to use for time delay estimation as we find in our experiments. To estimate critical times T_c of transition from the plateau region to the growth region, we approximate the growing region by a quadratic

function on the loglog scale. Specifically, we assume that $\ln T \approx a_2 (\ln \|E_R\|_\infty)^2 + a_1 \ln \|E_R\|_\infty + a_0 \equiv f(\ln \|E_R\|_\infty)$, where coefficients a_0 , a_1 , and a_2 are determined in the least squares sense. The resulting quadratic function $f(\ln \|E_R\|_\infty)$ is then evaluated at the value of $\|E_R\|_\infty$ at $T = 0$ that is assumed to be the “most causal” time. By taking exponential function of the result, we find a critical transition time T_c for a given M . This procedure produces estimates of the time delay T_0 for various values of M . The graph of the critical transition times T_c as a function of M is shown in Fig. 4. One can clearly see that the critical times approach the exact time delay $T_0 = 0.25$ as M increases. A good approximation of T_0 is achieved at $M = 800$. The values

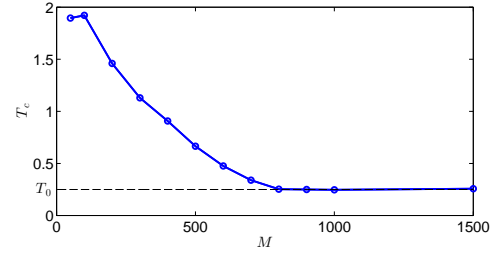


Fig. 4. Critical transition times T_c in the four-pole example that approach T_0 as M increases. The dashed line corresponds to the exact delay $T_0 = 0.25$.

of T_c for $M \geq 200$ are presented in Table I. The results indicate that the approximations become more accurate as M increases. The error with $M = 900$ is less than 1%. At the same time, the error with $M = 1500$ is about 3%, which is due to the fact that the results in this case are more affected by the filtering of singular values. In the cases when M is high and the resulting error is not flat for $T < T_0$, instead of evaluating a fitted quadratic curve at the value of $\|E_R\|_\infty$ at $T = 0$ we evaluate it at ξ , the threshold of filtering singular values, to avoid using results affected by filtering.

M	T_c	M	T_c
200	1.4604	700	0.3394
300	1.1294	800	0.2529
400	0.9077	900	0.2497
500	0.6655	1000	0.2472
600	0.4759	1500	0.2576

TABLE I
CRITICAL TRANSITION TIMES T_c IN THE FOUR-POLE EXAMPLE THAT APPROACH $T_0 = 0.25$ AS M INCREASES.

In practice the number N of samples of the transfer function $H(w)$ is usually limited, which sets the bound for number $M = N$ of Fourier coefficients, so it may not always be possible to use large enough M to obtain critical time T_c close enough to the actual time delay T_0 . A good method should be capable of producing an accurate approximation of T_0 even with a small number of data points. We achieve this by employing another approach for time delay estimation. Using the obtained fitted quadratic error curves, we extrapolate

them to the value ξ of filtering of singular values, which is typically chosen to be close to the machine precision. This corresponds to finding time T at which the error reaches the value ξ . This choice is natural since the errors below ξ are most likely affected by filtering and may not be accurate enough to use. The results of such extrapolation are shown in Fig. 5 for $M = 200, 400, 600$ and 800 . An intersection of the extrapolated curve corresponding to $M = 200$ is at a value $T = 0.45451$, which is a bit far from the exact $T_0 = 0.25$. At the same time, intersections of extrapolated curves with higher values of M are much closer – see Table II for details. Results

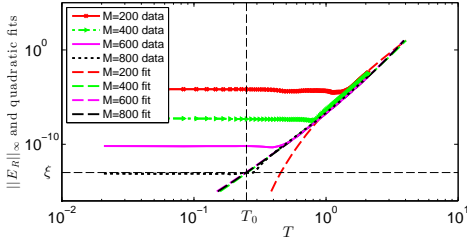


Fig. 5. $\|E_R\|_\infty$ in the four-pole example with $M = 200, 400, 600$ and 800 together with their extrapolated quadratic fits. Vertical dashed line indicates the exact time delay $T_0 = 0.25$, while horizontal dashed line indicates the level of filtering of singular values given by $\xi = 10^{-13}$.

M	T_0 approximation	M	T_0 approximation
200	0.45451	700	0.24734
300	0.27235	800	0.24969
400	0.25297	900	0.24974
500	0.25053	1000	0.24724
600	0.24633	1500	0.25759

TABLE II
APPROXIMATIONS OF $T_0 = 0.25$ IN THE FOUR-POLE EXAMPLE USING
EXTRAPOLATION.

shown in this table indicate that as M increases, extrapolated quadratic curve intersect the horizontal line the value ξ at times closer to T_0 . Obtained approximations of T_0 can be averaged producing $T_0 \approx 0.24805$. The approach with extrapolation provides a faster convergence and good approximations of T_0 even for small values of M , i.e. less data points are needed to approximate T_0 .

We also consider the effect of noise on the time delay estimation. To study this, we impose a sine perturbation

$$a \sin(10\pi x) \quad (18)$$

of various amplitudes a that we add to $\text{Re } H$, while keeping $\text{Im } H$ unchanged. We choose $N = 800$ and vary a from 10^{-10} to 10^{-3} . The reconstruction error E_R with no perturbation for early times $T < T_0$ is of the order of 10^{-13} , as shown in Fig. 6, that corresponds to the level of filtering of singular values. When the perturbation is added, the reconstruction errors for $T < T_0$ are higher and approximately of the order of a . Once some critical transition time greater than T_0 is

passed, reconstruction errors start growing and they grow at the same rate and coincide almost perfectly with each other. This observation suggests that the proposed approach can also be used in the cases when data have a noise, which is typical in real-life applications, when data have either measurement or simulation errors. For noise with a smaller amplitude, the

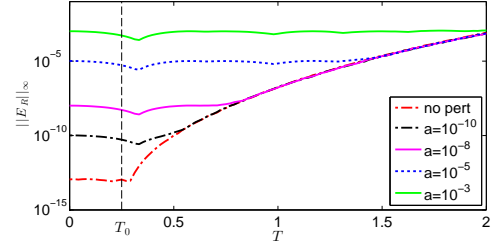


Fig. 6. Evolution of $\|E_R\|_\infty$ in the four-pole example with added sine perturbation $a \sin(10\pi x)$. The dashed line corresponds to the exact delay $T_0 = 0.25$.

region close to T_0 will be less affected by noise and a bigger growing region will be available for fitting, so we expect better accuracy of time delay estimation in such cases. When more noise in data is present, less growing region will be available for fitting and extrapolation of fitted quadratic error curves may be less accurate. We demonstrate this by considering two cases: with $a = 10^{-5}$ (noisier case) and $a = 10^{-8}$ (less noisy case). The error curves with a higher amplitude $a = 10^{-5}$ are

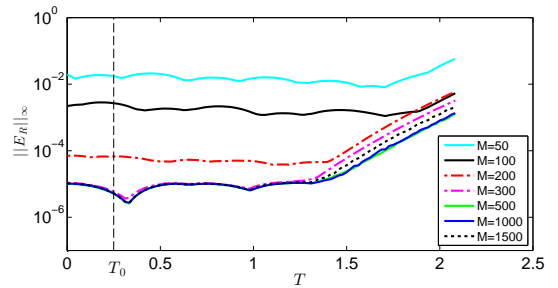


Fig. 7. Evolution of $\|E_R\|_\infty$ in the four-pole example with the added perturbation $10^{-5} \sin(10\pi x)$. The dashed line corresponds to the exact delay $T_0 = 0.25$.

presented in Fig. 7. It is clear that the error does not become smaller than 10^{-5} as $M \geq 300$ gets larger because of the noise. We use available growing regions and extrapolate fitted error curves to find their intersection with the horizontal line with value ξ . This gives us time T when the error reaches the value ξ for each considered M . The results of such extrapolation for $M = 200, 400, 600$ and 800 are shown in Fig. 8. Clearly, extrapolated error curves reach value ξ at times around T_0 but not close enough to T_0 and without established convergence but rather in a spread-out manner around T_0 . Approximations of T_0 for values of M that we investigated are shown in Table III. Averaging these approximations we obtain $T_0^{(aver)} = 0.26586$. The extrapolated curves can be

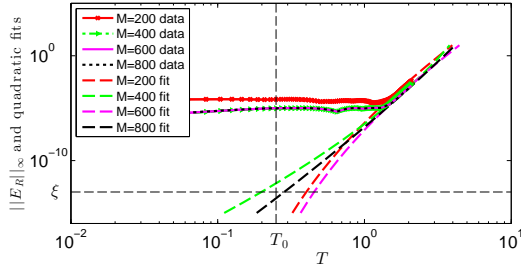


Fig. 8. Error curves $\|E_R\|_\infty$ in the four-pole example with the added perturbation $10^{-5} \sin(10\pi x)$ and $M = 200, 400, 600$ and 800 together with their extrapolated quadratic fits. Vertical dashed line indicates the exact time delay $T_0 = 0.25$, while horizontal dashed line indicates the level of filtering of singular values given by $\xi = 10^{-13}$.

M	T_0 estimate	M	T_0 estimate
200	0.40158	700	0.39113
300	0.25578	800	0.28392
400	0.19863	900	0.26543
500	0.14311	1000	0.20293
600	0.45358	1500	0.32837

TABLE III
APPROXIMATIONS OF T_0 IN THE FOUR-POLE EXAMPLE WITH PERTURBATION $10^{-5} \sin(10\pi x)$ USING EXTRAPOLATIONS WITH ORIGINAL FITTING REGIONS FOR VARIOUS M . THE EXACT VALUE $T_0 = 0.25$, AVERAGED VALUE $T_0^{(aver)} = 0.26586$.

made more focused around T_0 by narrowing down the fitted region. Results of this procedure are shown in Fig. 9. This improves a little an average time delay to $T_0^{(aver)} = 0.24216$.

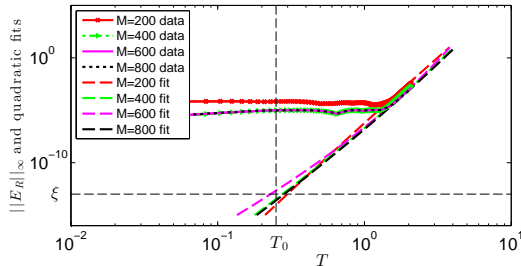


Fig. 9. $\|E_R\|_\infty$ in the four-pole example with the added perturbation $10^{-5} \sin(10\pi x)$ and $M = 200, 400, 600$ and 800 together with their extrapolated quadratic fits constructed using more narrow fitting region. Vertical dashed line indicates the exact time delay $T_0 = 0.25$, while horizontal dashed line indicates the level of filtering of singular values given by $\xi = 10^{-13}$.

Next we show results when a smaller noise of amplitude $a = 10^{-8}$ is added. The evolution of $\|E_R\|_\infty$ as T increases is shown in Fig. 10. We can see that the plateau error region in this case is at about 10^{-9} level, so the error growth region is bigger than in the previous case, which should make fitting and extrapolation more accurate. Indeed, extrapolated quadratic curves intersect the horizontal line with value ξ in a more localized region about T_0 as shown in Fig. 11,

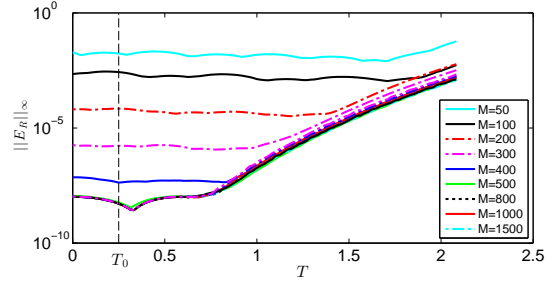


Fig. 10. Evolution of $\|E_R\|_\infty$ in the four-pole example with the added perturbation $10^{-8} \sin(10\pi x)$ of smaller amplitude. The dashed line corresponds to the exact delay $T_0 = 0.25$.

while averaging of obtained approximation to T_0 produces $T_0^{(aver)} = 0.25436$, which is more accurate than in the case with a higher amplitude $a = 10^{-5}$.

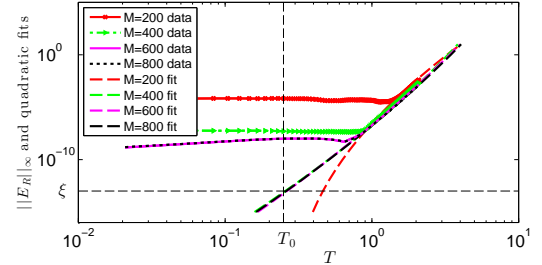


Fig. 11. $\|E_R\|_\infty$ in the four-pole example with the added perturbation $10^{-8} \sin(10\pi x)$ and $M = 200, 400, 600$ and 800 together with their extrapolated quadratic fits. Vertical dashed line indicates the exact time delay $T_0 = 0.25$, while horizontal dashed line indicates the level of filtering of singular values given by $\xi = 10^{-13}$.

M	T_0 estimate	M	T_0 estimate
200	0.46392	700	0.25502
300	0.27635	800	0.26081
400	0.25683	900	0.2444
500	0.26798	1000	0.25582
600	0.26391	1500	0.25292

TABLE IV
APPROXIMATIONS OF T_0 IN THE FOUR-POLE EXAMPLE WITH PERTURBATION $10^{-8} \sin(10\pi x)$ USING EXTRAPOLATIONS FOR VARIOUS M . THE EXACT VALUE $T_0 = 0.25$, AVERAGED VALUE $T_0^{(aver)} = 0.25436$.

B. Transmission Line Example

We consider a uniform transmission line segment with the following per-unit-length parameters: $L = 7.574$ nH/inch, $C = 2.61166$ pF/inch, $R = 16.278$ mΩ/inch, $G = 5.58$ μS/inch and length $\mathcal{L} = 5$ inches. The frequency is sampled on the interval $(0, 5.0]$ GHz. The scattering matrix of the

structure is computed using Matlab function `rlgc2s`. We consider the element $\tilde{H}(w) = S_{11}(w)$ and impose the time delay $T_0 = 1.25$ ns by multiplying $\tilde{H}(w)$ by $\exp(-iwT_0)$ to get the delayed transfer function $H(w) = \exp(-iwT_0)\tilde{H}(w)$. The real and imaginary parts of $H(w)$ are given in Fig. 12. The

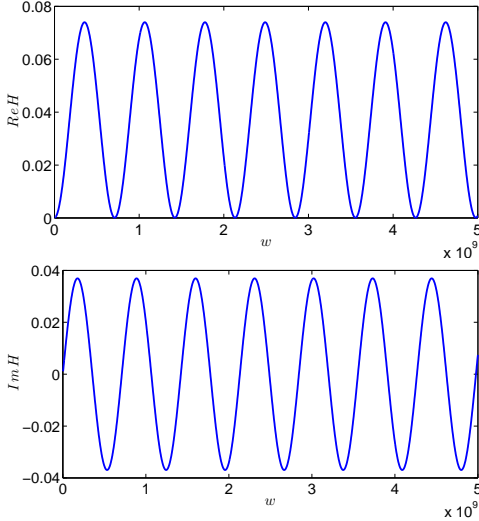


Fig. 12. $\text{Re } H(w)$ and $\text{Im } H(w)$ in the transmission line example.

error curves for different M are shown in Fig. 13 indicating that the reconstruction error decreases quickly with M and reaches the level close to machine precision at $M = 600$. Constructing fitted quadratic error curves and finding their

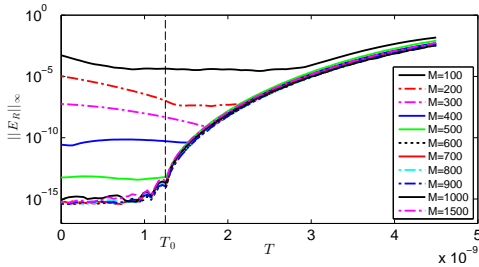


Fig. 13. Evolution of $\|E_R\|_\infty$ in the transmission line example as M varies. Vertical dashed line indicates the time delay $T_0 = 1.25$ ns.

intersections with $\|E_R\|_\infty$ at $T = 0$ or finding times when these fitted error curves reach the value ξ of the error for $M \geq 600$, we get a sequence of critical transition times T_c , that we show in Fig. 14. Clearly, critical times T_c converge to T_0 and provide a good approximation of T_0 for $M \geq 500$. Using an alternative approach when we extrapolate the fitted quadratic error curves to find their intersections with the error threshold ξ , we find approximations of T_0 . Some of these curves for $M = 200, 400, 600$ and 800 are depicted in Fig. 15. Approximations of T_0 using extrapolation procedure for various values of M ranging from $M = 200$ to 1500 are given in Table V. A good approximation of T_0 is obtained even with $M = 300$. As before, approximations of T_0 become better as M increases, but for very large values of $M \geq 1000$ when the reconstruction error falls below the filtering threshold ξ and

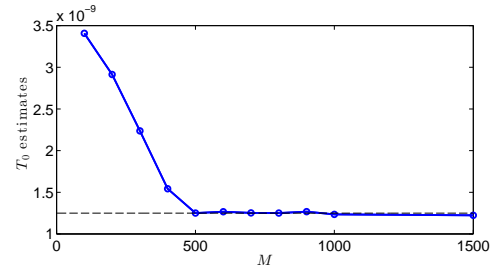


Fig. 14. Estimation of the delay time in the transmission line example using critical transition times T_c as M varies. The dashed line corresponds to the exact delay $T_0 = 1.25$ ns.

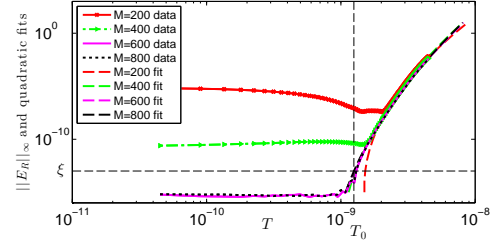


Fig. 15. $\|E_R\|_\infty$ in the transmission line example with $M = 200, 400, 600$ and 800 together with their quadratic fits. Vertical dashed line indicates the exact time delay $T_0 = 1.25$ ns, while horizontal dashed line indicates the level of filtering of singular values given by $\xi = 10^{-13}$.

filtering affects the results more, extrapolation becomes less accurate. Averaging obtained approximations of T_0 produces $T_0^{(aver)} = 1.2498$ ns, that is very close to the exact value $T_0 = 1.25$ ns.

M	T_0 estimate (in ns)	M	T_0 estimate (in ns)
200	1.5194	700	1.2531
300	1.3147	800	1.2512
400	1.2793	900	1.2678
500	1.2506	1000	1.2348
600	1.2668	1500	1.2242

TABLE V
APPROXIMATIONS OF T_0 IN THE TRANSMISSION LINE EXAMPLE USING EXTRAPOLATIONS FOR VARIOUS M . THE EXACT VALUE $T_0 = 1.25$ NS, AVERAGED VALUE $T_0^{(aver)} = 1.2498$ NS.

C. Dawson's Integral Example

We consider here another analytic example [23] modeled by the transfer function

$$H(w) = e^{-iwT_0} \tilde{H}(w)$$

where

$$\tilde{H}(w) = e^{-w^2} - \frac{2i}{\sqrt{\pi}} D(w),$$

$D(w)$ is Dawson's integral

$$D(w) = e^{-w^2} \int_0^w e^{t^2} dt = \frac{\sqrt{\pi}}{2} e^{-w^2} \text{erfi}(w)$$

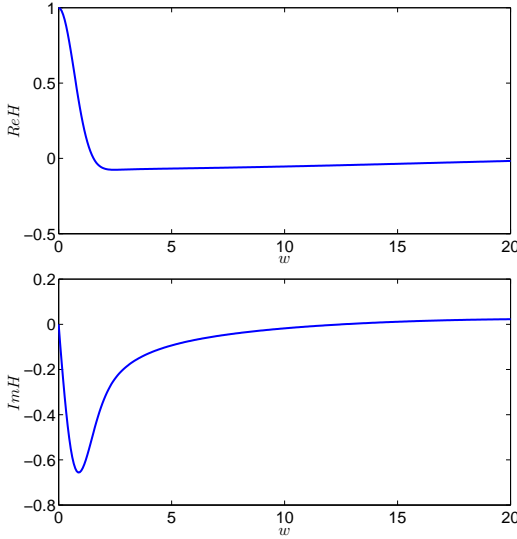


Fig. 16. $\text{Re } H(w)$ and $\text{Im } H(w)$ in the Dawson's integral example using $N = 300$ sample points.

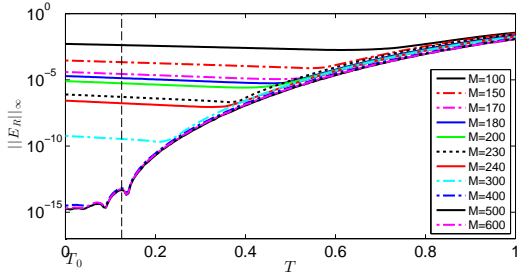


Fig. 17. $\|E_R\|_\infty$ in the Dawson's integral example as M varies. Vertical dashed line indicates the time delay $T_0 = 0.125$.

and $\text{erfi}(w)$ is the imaginary error function. Since [38]³

$$\mathcal{H}[\text{Re } \tilde{H}] = \mathcal{H}(e^{-w^2}) = \frac{2}{\sqrt{\pi}} D(w) = -\text{Im } \tilde{H},$$

function $\tilde{H}(w)$ is causal. Hence, the function $H(w)$ is a causal function delayed with offset T_0 . We use $T_0 = 0.125$ and sample $H(w)$ on $[0, w_{max}]$ with $w_{max} = 20$ using various numbers of points ranging from $N = 100$ to 600 . Real and imaginary parts of H are shown in Fig. 16. The evolution of $\|E_R\|_\infty$ for various M is shown in Fig. 17, where it is clear that critical transition times approach T_0 . Constructing fitted quadratic error curves and extrapolating them to find their intersections with the horizontal line corresponding to the error value ξ produces a set of approximation of T_0 , shown in Table VI. Averaging obtained approximations of T_0 for $M \geq 200$, once some convergence is established, gives $T_0^{(aver)} = 0.12528$.

It is interesting to note behavior of the relative error E_R^{rel} in this example. The evolution of its ∞ norm is shown in Fig. 18. It is clear that all profiles even for small values of M have a unique local maximum at $T = T_0$. 2-norm has a similar

³Please note that we use an opposite sign in the definition of the Hilbert transform than in [38] and [23].

M	T_0 estimate	M	T_0 estimate
150	0.16735	240	0.12362
170	0.13116	300	0.12661
180	0.12964	400	0.12233
200	0.12753	500	0.12578
230	0.12333	600	0.12414

TABLE VI
APPROXIMATIONS OF T_0 IN THE DAWSON'S INTEGRAL EXAMPLE USING EXTRAPOLATIONS OF FITTED ERROR CURVES FOR VARIOUS M . THE EXACT VALUE $T_0 = 0.125$, AVERAGED VALUE FOR M RANGING FROM 200 TO 600 IS $T_0^{(aver)} = 0.12528$.

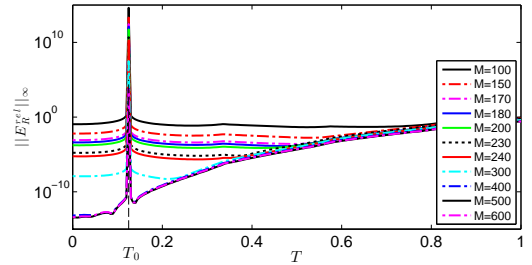


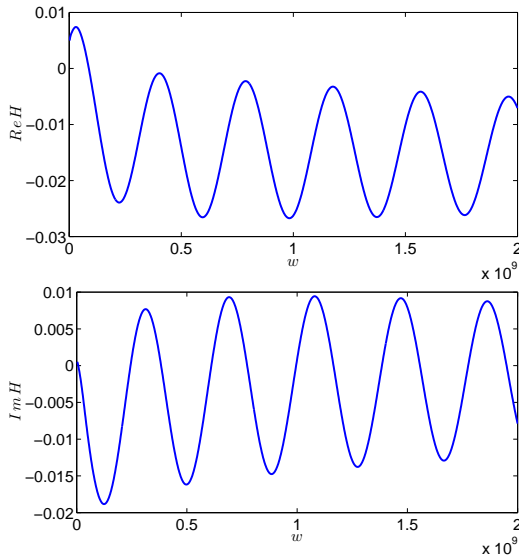
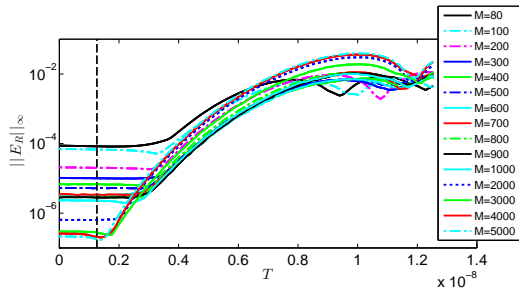
Fig. 18. Evolution of the relative error $\|E_R^{rel}\|_\infty$ in the Dawson's integral example as M varies. Vertical dashed line indicates the time delay $T_0 = 0.125$.

behavior. Even though the behavior of the relative error E_R^{rel} can be used to determine the time delay in this example, we did not find the same pronounced behavior in other examples we considered. At the same time, extrapolating fitted quadratic curves of ∞ norms of the absolute error E_R was a robust approach in all examples we considered.

D. Stripline Example

We simulated an asymmetric stripline modeled in [37] with length $L = 8$ in, width $W = 14$ mils, distances from the trace to reference planes $H_1 = 10$ mils, $H_2 = 20$ mils, substrate dielectric Megtron6-1035, Laminate with a dielectric constant $\epsilon_r = 3.45$ using a Cadence software tool with FEM full-wave field solver. The stripline was simulated on $[0, w_{max}]$ with $w_{max} = 2$ GHz. We analyzed element $H(w) = S_{11}(w)$ of the transfer matrix. The real and imaginary parts of H are shown in Fig. 19. The evolution of $\|E_R\|_\infty$ for various M is depicted in Fig. 20. Even for high values of M , the error in causality does not go to machine precision and instead levels off around 10^{-6} . This indicates that our finite element simulation results are accurate only within $10^{-7} - 10^{-6}$. For causality characterization, this implies that data have noise/approximation errors with amplitude around $10^{-7} - 10^{-6}$. Graphs of $\|E_R\|_\infty$ suggest that for $M \leq 2000$, the error is dominated by Fourier series approximation error, while for higher of M , the error is dominated by the noise/approximation errors from the finite element method.

In this example, the time delay was estimated using a closed form microwave theory approximation as $T_0 = 8 \times$

Fig. 19. $\text{Re } H$ and $\text{Im } H$ in the stripline example with $N = 1000$.Fig. 20. $\|E_R\|_\infty$ in the stripline example for various M . Vertical dashed line indicates the closed form microwave theory time delay approximation $T_0 = 1.25809$ ns.

$0.0254/(c_0/\sqrt{\epsilon_r}) = 1.25809$ ns, where $c_0 = 3 \times 10^8$ m/s is the speed of light, 0.0254 is a conversion factor to convert from inches to meters. The error curves were fitted to quadratic curves as explained above. Because of relatively high errors in data, the fitted regions are not long enough. Besides, there is more nonlinear behavior of the error curves for high values of $T > T_0$. All this makes it difficult to estimate the time delay as shown in Fig. 21. As can be seen, extrapolated quadratic curves do not focus at T_0 but instead spread out around T_0 similar to the four-pole example with an imposed noise considered in Section V-A. This problem can be corrected

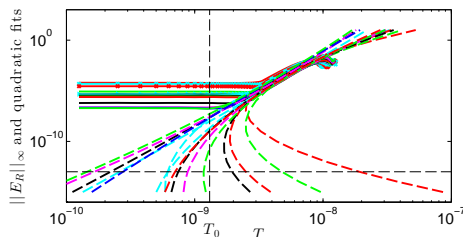
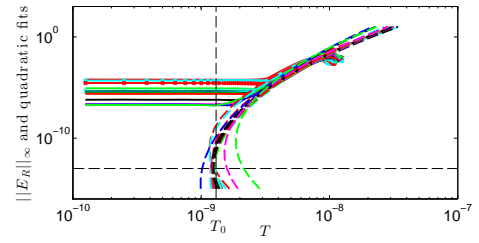


Fig. 21. Extrapolated quadratic curves based on initial fitting range in the stripline example.

Fig. 22. Extrapolated quadratic curves based on more narrow fitting range in the stripline example. The average time delay is $T_0^{(aver)} = 1.2669$ ns.

by decreasing the fitting range and going more away from transition regions. The results are shown in Fig. 22. The approximations of T_0 are given in Table VII. Averaging them for values of M up to 3000 produces $T_0^{(aver)} = 1.2669$ ns, that agrees well with an analytically estimated time delay using a closed form formula. As in other examples, results with very high values of $M > 3000$, that are more affected by noise and approximation errors in data, are less accurate.

M	T_0 estimate (in ns)	M	T_0 estimate (in ns)
80	1.266	700	1.1987
100	1.2312	800	1.2179
200	1.2553	900	1.2593
300	1.2797	1000	1.2205
400	1.2826	2000	1.246
500	1.2413	3000	1.5878
600	1.1833	4000	1.0168

TABLE VII
APPROXIMATIONS OF T_0 IN THE STRIPLINE EXAMPLE USING
EXTRAPOLATIONS OF FITTED QUADRATIC ERROR CURVES FOR VARIOUS
 M . THE CLOSED FORM APPROXIMATION OF THE TIME DELAY IS
 $T_0 = 1.25809$ NS, AVERAGED VALUE FOR M RANGING TO UP TO 3000 IS
 $T_0^{(aver)} = 1.2669$ NS.

VI. CONCLUSIONS

We proposed a new method for time delay extraction from tabulated frequency responses. The approach uses the spectrally accurate causality enforcement technique constructed using SVD-based causal Fourier continuations, that was recently developed by the authors. The time delay is incorporated to the causality characterization approach by introducing a linear varying phase factor to the system of equations that defines Fourier coefficients. Varying time until a threshold time, that depends on the maximum frequency at which the transfer function is available, results in the reconstruction error between the given data and their causal Fourier continuations to go from an almost constant small value to a rapidly growing function at some critical transition time. The critical transition times depend on resolution and approach the time delay as resolution increases. Several sets of frequency responses with increasing resolution can be used to establish convergence and get an approximation of the time delay. Alternatively, when

only a limited number of samples is available, a growing portion of the error curve can be extrapolated to find an approximation of the time delay. The method is applicable to data that have noise or other approximation errors. A few sets of frequency responses can be used to improve the accuracy of time delay approximation by averaging the obtained results. The technique can be extended for multi-port and mixed mode networks. The performance of the method is demonstrated using several analytic and simulated examples, including data with noise, for which time delay is known exactly or can be estimated using other approaches.

ACKNOWLEDGMENT

The authors are grateful to Dr. Linh V. Nguyen for valuable discussions on the Fourier transform. The work was supported by the Micron Foundation. The author L.L.B. would also like to acknowledge the availability of computational resources made possible through the National Science Foundation Major Research Instrumentation Program, grant 1229766.

APPENDIX

ERROR ANALYSIS OF CAUSALITY CHARACTERIZATION METHOD BASED ON CAUSAL FOURIER CONTINUATIONS

In this section, we provide an upper bound of the reconstruction error between a given transfer function $H(x)$ and its causal Fourier continuation $\mathcal{C}(H)(x)$ in the presence of noise ϵ in data.

Denote by \hat{H}_M any function of the form

$$\hat{H}_M(x) = \sum_{k=1}^M \hat{\alpha}_k \phi_k(x) \quad (19)$$

where $\phi_k(x) = e^{-\frac{2\pi i}{b} kx}$, $k = 1, \dots, M$.

Let $A = U\Sigma V^*$ be the full SVD decomposition [34] of the matrix A with entries $A_{kj} = \phi_k(x_j)$, $j = 1, \dots, N$, $k = 1, \dots, M$, where U is an $N \times N$ unitary matrix, Σ is an $N \times M$ diagonal matrix of singular values σ_j , $j = 1, \dots, p$, $p = \min(N, M)$, V is an $M \times M$ unitary matrix with entries V_{kj} , and V^* denotes the complex conjugate transpose of V .

The following result is true [4].

Theorem : Consider a rescaled transfer function $H(x)$ defined by symmetry on $\Omega = [-0.5, -a] \cup [a, 0.5]$, where $a = 0.5 \frac{w_{min}}{w_{max}}$, whose values are available at points $x_j \in \Omega$, $j = 1, \dots, N$. Then the error in approximation of $H(x)$, that is known with some error ϵ , by its causal Fourier continuation $\mathcal{C}(H)(x)$ defined in (7) on a wider domain $\Omega^c = [-b/2, b/2]$, $b \geq 1$, has the upper bound

$$\|H - \mathcal{C}(H + \epsilon)\|_{L_2(\Omega)} \leq (1 + \Lambda_2 \sqrt{N(M - K)}) \times \left(\|H - \hat{H}_M\|_{L_\infty(\Omega)} + \|\epsilon\|_{L_\infty(\Omega)} \right) + \Lambda_1 \sqrt{K/b} \|\hat{H}_M\|_{L_\infty(\Omega^c)}$$

and holds for all functions of the form (19). Here

$$\Lambda_1 = \max_{j: \sigma_j < \xi} \|v_j(x)\|_{L_2(\Omega)}, \quad \Lambda_2 = \max_{j: \sigma_j > \xi} \frac{\|v_j(x)\|_{L_2(\Omega)}}{\sigma_j},$$

and functions $v_j(x) = \sum_{k=1}^M V_{kj} \phi_k(x)$ are each an up to M term causal Fourier series with coefficients given by the j th

column of V ; K denotes the number of singular values that are discarded, i.e. the number of j for which $\sigma_j < \xi$, where ξ is the cut-off tolerance.

It can be seen that constants Λ_1 , Λ_2 and K depend only on the continuation parameters N , M , b and ξ as well as location of discrete points x_j , and not on the function H .

For brevity, we can write the above error estimate as

$$\|H - \mathcal{C}(H + \epsilon)\|_{L_2(\Omega)} \leq \epsilon_F + \epsilon_n + \epsilon_T.$$

Here

$$\epsilon_F \equiv (1 + \Lambda_2 \sqrt{N(M - K)}) \|H - \hat{H}_M\|_{L_\infty(\Omega)}$$

is the error due to a causal Fourier series approximation and it decays at least as fast as $\mathcal{O}(M^{-k+1})$, k is the smoothness order of $H(x)$, which can be estimated numerically using reconstruction errors with different resolution (see [4]).

$$\epsilon_T = \Lambda_1 \sqrt{K/b} \|\hat{H}_M\|_{L_\infty(\Omega^c)},$$

that is the error due to the truncation of singular values. It is typically small and close to the cut-off value ξ .

$$\epsilon_n = (1 + \Lambda_2 \sqrt{N(M - K)}) \|\epsilon\|_{L_\infty(\Omega)}$$

is the error due to noise ϵ in data. Numerical experiments reveal that ϵ_n has the order of noise ϵ in data.

REFERENCES

- [1] ABOUTALEB, H. A., BARANNYK, L. L., ELSHABINI, A., AND BARLOW, F. Causality enforcement of DRAM package models using discrete Hilbert transforms. In *2013 IEEE Workshop on Microelectronics and Electron Devices, WMED 2013* (2013), pp. 21–24.
- [2] BARANNYK, L. L., ABOUTALEB, H. A., ELSHABINI, A., AND BARLOW, F. Causality Enforcement of High-Speed Interconnects via Periodic Continuations. In *47th International Symposium on Microelectronics, IMAPS 2014, October 14-16, 2014* (2014), pp. 236–241.
- [3] BARANNYK, L. L., ABOUTALEB, H. A., ELSHABINI, A., AND BARLOW, F. Causality verification using polynomial periodic continuations. *J. Microelectron. Electron. Packag.* 11, 4 (2014), 181–196.
- [4] BARANNYK, L. L., ABOUTALEB, H. A., ELSHABINI, A., AND BARLOW, F. Spectrally accurate causality enforcement using SVD-based Fourier continuations. *IEEE Trans. Comp. Packag. Manuf. Techn.* 5, 7 (2015), 991–1005.
- [5] BARANNYK, L. L., TRAN, H. H., NGUYEN, L. V., ELSHABINI, A., AND BARLOW, F. Time delay estimation using SVD-based causal Fourier continuations for high speed interconnects. In *2015 IEEE 24th Conference on Electrical Performance of Electronic Packaging and Systems, Oct. 25-28, 2015, in San Jose, California, USA* (2015), p. accepted.
- [6] CHAREST, A., NAKHLA, M. S., ACHAR, R., SARASWAT, D., SOVEIKO, N., AND ERDIN, I. Time Domain Delay Extraction-Based Macromodeling Algorithm for Long-Delay Networks. *IEEE Trans. Adv. Packag.* 33, 1 (2010), 219–235.
- [7] CHAREST, A., SARASWAT, D., NAKHLA, M., ACHAR, R., AND SOVEIKO, N. Compact macromodeling of high-speed circuits via delayed rational functions. *IEEE Microw. Compon. Lett.* 17, 12 (2007), 828–830.
- [8] CHEN, J., BENESTY, J., AND HUANG, Y. A. Time delay estimation in room acoustic environments: An overview. *EURASIP J Appl Signal Processing* (2006).
- [9] CHINEA, A., TRIVERIO, P., AND GRIVET-TALOCIA, S. Delay-Based Macromodeling of Long Interconnects From Frequency-Domain Terminal Responses. *IEEE Trans. Adv. Packag.* 33, 1 (2010), 246–256.
- [10] DE MARCHI, L., MARZANI, A., CAPORALE, S., AND SPECIALE, N. Ultrasonic Guided-Waves Characterization With Warped Frequency Transforms. *IEEE Trans. Ultrason. Ferroelectr. Freq. Control* 56, 10 (2009), 2232–2240.

- [11] DE TOMMASI, L., AND GUSTAVSEN, B. Low order transmission line modeling by modal decomposition and minimum phase shift fitting. In *10th IEEE Workshop on Signal Propagation on Interconnects, Proceedings* (2006), pp. 89–92. 10th IEEE Workshop on Signal Propagation on Interconnects, Berlin, Germany, May 09-12, 2006.
- [12] DESCHRIJVER, D., AND DHAENE, T. Rational modeling of spectral data using orthonormal vector fitting. In *SIGNAL PROPAGATION ON INTERCONNECTS, PROCEEDINGS* (2005), pp. 111–114. 9th IEEE Workshop on Signal Propagation on Interconnects, Garmisch Partenkirchen, GERMANY, MAY 10-13, 2005.
- [13] DESCHRIJVER, D., HAEGEMAN, B., AND DHAENE, T. Orthonormal vector fitting: A robust macromodeling tool for rational approximation of frequency domain responses. *IEEE Trans. Adv. Packag.* 30, 2 (2007), 216–225.
- [14] GRENNBERG, A., AND SANDELL, M. Estimation of Subsample Time-Delay Differences in Narrow-Band Ultrasonic Echoes Using the Hilbert Transform Correlation. *IEEE Trans Ultrason Ferroelectr Freq Control* 41, 5 (1994), 588–595.
- [15] GRIVET-TALOCIA, S. Package macromodeling via time-domain vector fitting. *IEEE Microw. Compon. Lett.* 13, 11 (2003), 472–474.
- [16] GRIVET-TALOCIA, S. Delay-based macromodels for long interconnects via time-frequency decompositions. In *Electrical Performance of Electronic Packaging* (2006), pp. 199–202. 15th IEEE Topical Meeting on Electrical Performance of Electronic Packaging, Scottsdale, AZ, Oct. 23-25, 2006.
- [17] GRIVET-TALOCIA, S., AND BANDINU, M. Improving the convergence of vector fitting for equivalent circuit extraction from noisy frequency responses. *IEEE Trans Electromagn. Compat.* 48, 1 (2006), 104–120.
- [18] GUSTAVSEN, B. Time delay identification for transmission line modeling. In *8th IEEE Workshop on Signal Propagation on Interconnects* (2004), pp. 103–106. Heidelberg, Germany, May 09-12, 2004.
- [19] GUSTAVSEN, B., AND SEMLYEN, A. Rational approximation of frequency domain responses by vector fitting. *IEEE Trans. Trans. Power Delivery* 14, 3 (1999), 1052–1061.
- [20] GUSTAVSEN, B., AND SEMLYEN, A. A robust approach for system identification in the frequency domain. *IEEE Trans. Trans. Power Delivery* 19, 3 (2004), 1167–1173.
- [21] HASSAB, J. C., AND BOUCHER, R. Probabilistic Analysis of Time-Delay Extraction by Cepstrum in Stationary Gaussian Noise. *IEEE Trans Inf Theory* 22, 4 (1976), 444–454.
- [22] KEPKO, L., AND KIVELSON, M. Generation of Pi2 pulsations by bursty bulk flows. *J. Geophys. Res. – Space Phys.* 104, A11 (1999), 25021–25034.
- [23] KNOCKAERT, L., AND DHAENE, T. Causality determination and time delay extraction by means of the eigenfunctions of the Hilbert transform. In *12th IEEE Workshop on Signal Propagation on Interconnects* (2008), pp. 19–22. Avignon, France, May 12-15, 2008.
- [24] LALGUDI, S. N., ENGIN, E., CASINOVI, G., AND SWAMINATHAN, M. Accurate transient simulation of interconnects characterized by band-limited data with propagation delay enforcement in a modified nodal analysis framework. *IEEE Trans. Electromagn. Compat.* 50, 3, 2 (2008), 715–729.
- [25] LI, M. C. A high precision Doppler radar based on optical fiber delay loops. *IEEE Trans. Antennas Propag.* 52, 12 (2004), 3319–3328.
- [26] LIM, H. B., NHUNG, N. T. T., LI, E.-P., AND THANG, N. D. Confocal microwave imaging for breast cancer detection: Delay-multiply-and-sum image reconstruction algorithm. *IEEE Trans. Biomed. Eng.* 55, 6 (2008), 1697–1704.
- [27] MANDREKAR, R., SRINIVASAN, K., ENGIN, E., AND SWMINATHAN, M. Causality enforcement in transient co-simulation of signal and power delivery networks. *IEEE Trans. Adv. Packag.* 30, 2 (2007), 270–278. 14th Conference on Electrical Performance of Electronic Packages, Austin, TX, 2005.
- [28] MANDREKAR, R., AND SWAMINATHAN, M. Delay extraction from frequency domain data for causal macro-modeling of passive networks. In *2005 International Symposium on Circuits and Systems (ISCAS), Japan, May 23-26, 2005* (2005), vol. 1–6, pp. 5758–5761.
- [29] MERCERAT, E. D., AND NOLET, G. On the linearity of cross-correlation delay times in finite-frequency tomography. *Geophys. J. Int.* 192, 2 (2013), 681–687.
- [30] NAKHLA, N. M., DOUNAVIS, A., ACHAR, R., AND NAKHLA, M. S. DEFACT: Delay extraction-based passive compact transmission-line macromodeling algorithm. *IEEE Trans. Adv. Packag.* 28, 1 (FEB 2005), 13–23. Conference on Electrical Performance of Electronic Packaging, Princeton, NJ, Oct. 26, 2003.
- [31] NUSSENZVEIG, H. M. *Causality and Dispersion Relations*. Academic Press, 1972.
- [32] PAPOULIS, A. *Signal Analysis*. McGraw-Hill College, 1977.
- [33] QUAZI, A. H. An Overview on the Time-Delay Estimate in Active and Passive Systems for Target Localization. *IEEE Trans Acoust Speech Signal Process* 29, 3 (1981), 527–533.
- [34] TREFETHEN, L. N., AND BAU III, D. *Numerical Linear Algebra*. SIAM: Society for Industrial and Applied Mathematics, 1997.
- [35] TSUCHIYA, Y., AND MIKI, Y. Delay time estimation using Hilbert transform and new extrapolation procedure. In *SICE 2004 Annual Conference, Vols 1-3* (2004), pp. 776–780. SICE 2004 Annual Conference, Sapporo, Japan, Aug, 04-06, 2005.
- [36] VANDERVEEN, M., VAN DER VEEN, A., AND PAULRAJ, A. Estimation of multipath parameters in wireless communications. *IEEE Trans Signal Process* 46, 3 (1998), 682–690.
- [37] WANG, C., DREWNIK, J. L., FAN, J., KNIGHTEN, J. L., SMITH, N. W., AND ALEXANDER, R. Transmission line modeling of vias in differential signals. In *2002 IEEE International Symposium on Electromagnetic Compatibility* (2002), pp. 249–252.
- [38] WEIDEMAN, J. A. C. Computing the Hilbert transform on the real line. *Math. Comp.* 64, 210 (1995), 745–762.
- [39] WILCOCK, W. S. D. Physical response of mid-ocean ridge hydrothermal systems to local earthquakes. *Geochem. Geophys. Geosyst.* 5 (2004).